1

2

Supporting Information for

3

On assessing ERA5 and MERRA2 representations of cold-air outbreaks across the Gulf Stream

4
5
6

7   Seethala Chellappan[1], Paquita Zuidema[1], Jim Edson[2], Michael Brunke[3], Gao Chen[4], Xiang-
8   Yu Li[5], David Painemal[4,6], Claire Robinson[4], Taylor Shingler[6], Michael Shook[6], Armin
9   Sorooshian[3,7], Lee Thornhill[6], Florian Tornow[8,9], Hailong Wang[5], Xubin Zeng[3], Luke
10 Ziemba[6]

11 [1]Rosenstiel School of Marine and Atmospheric Science, University of Miami, Miami, FL
12 [2]Woods Hole Oceanographic Institution, Woods Hole, MA
13 [3]Department of Hydrology and Atmospheric Sciences, University of Arizona, Tucson, AZ
14 [4]Science Systems and Applications, Inc., Hampton, VA
15 [5]Pacific Northwest National Laboratory, Richland, WA
16 [6]NASA Langley Research Center, Hampton, VA
17 [7]Department of Chemical and Environmental Engineering, University of Arizona, Tucson,
18 AZ
19 [8]Earth Institute, Columbia University, New York City, NY
20 [9]NASA Goddard Institute for Space Sciences, New York City, NY
21
22

23

24

25

26   **Contents of this file**
27
28   Datasets and Method
29   Tables S1 to S3
30   Figures S1 to S5
31
32
33
34

35
36
37

Datasets and Method:

The CLIMODE mooring sampled along the northern periphery of the Gulf Stream in late January-mid February 2006 and again in late March-April 2006, and was otherwise within warmer waters (Weller et al., 2012), with its position relative to the Gulf Stream shown using GHRSST in Fig. S1. The anchor line maintains the buoy within 5-7 km of its nominal position. The Air-Sea Interaction Meteorological system made continuous measurements of temperature (T), relative humidity (RH) and wind speed (WS) at about 3 m above the waterline and measured the SST at a depth of 0.89 m. Radiometers provided downwelling solar and IR radiative fluxes used to estimate the 'skin' sea surface temperature (Fairall et al., 1996). A Direct Covariance Flux System allowed direct covariance computations of buoyancy fluxes (and surface wind stresses; Edson et al., 2013).

GHRSST optimally integrates cloud-penetrating microwave SST data with infrared data of a higher spatial resolution into a daily global SST dataset. We use a 9 km v5.0 MW_IR OISST product available from Remote Sensing Systems.

The reference atmospheric structure information comes from precalibrated NCAR (National Centre for Atmospheric Research) Dropsonde 94 (NRD94s; Wick et al., 2018), released from the NASA Langley Beechcraft UC12 research aircraft at an approximate flight altitude of 9 km. Pressure, temperature and humidity data are returned at 2 Hz, and of winds at 4 Hz, corresponding to a vertical resolution of 6-15 m. The pressure, temperature, humidity and wind speed are resolved to 0.1 hPa, 0.1^{0}C, 1% and 0.1 m s^{-1}, respectively, with a standard deviation of differences between two successive repeated calibrations of 0.4 hPa, 0.2^{0}C, 2% and 0.2 m s^{-1}, respectively.

ERA5 is the fifth-generation global atmospheric reanalysis developed by the European Centre of Medium-range Weather Forecast (ECMWF), described comprehensively within Hersbach et al., (2020). ERA5 relies on a 12-hr 4D-var Integrated Forecasting System (IFS) cycle 41R2 data assimilation, with data available every hour at a horizontal resolution of 31 km, gridded to 0.25^{0}. The ERA5 atmospheric model is coupled with a land surface and a wave model, with internal computations encompassing 137 vertical levels, of which 37 are output, including the lowest level at 10 m. ERA5 estimates of the temperature and specific humidity at 2 m altitude (T_{2m} and q_{2m}), developed using Monin-Obukhov theory to relate the skin sea surface temperature and its saturated specific humidity to the 10 m model level,

69 support explicit comparisons to buoy measurements. Rivas and Stoffelen, (2019) document

70 improved mid-latitude storm track surface wind representations compared to the previous

71 ERA-Interim, attributed to a higher vertical resolution (137 vs 60 model levels).

72   MERRA2 (Modern Era Retrospective analysis for Research and Applications;

73 Bosilovich et al., 2015) relies on the Goddard Earth Observing System (GEOS-5.12)

74 atmospheric global model (Molod et al., 2015) combined with the Gridpoint Statistical

75 Interpolation data assimilation system (Wu et al. 2002). MERRA2 assimilates microwave

76 and infrared radiances and select retrievals from polar-orbiters and geostationary satellites,

77 including aerosol optical depth. Daily 0.25^ox0.25^o Reynolds SSTs (Reynolds et al., 2007)

78 were prescribed until March 2006, and thereafter, high resolution satellite-derived daily SSTs

79 similar to the OISSTs used by ERA5. Recent relevant improvements include an improved

80 relationship between the ocean surface roughness and ocean surface stress (Molod et al.,

81 2015). The change from MERRA to MERRA2 reduces surface wind speeds in the

82 ACTIVATE region, by approximately 2 m s^{-1}, but surface turbulent fluxes are marginally

83 affected, and a change in the critical relative humidity for cloud condensation also produce

84 little change in the boundary layer q, both just for the ACTIVATE region (Molod et al.,

85 2015).

86   The bulk fluxes are calculated from the dropsondes using the TOGA-COARE v.3.5

87 bulk flux algorithm. This relies on Monin-Obukhov similarity theory as:

88
$$Q_H = \rho \, C_H \, U \left(S_{surf} - S_{2m} \right) \qquad \text{------------- (S1)}$$

89
$$Q_E = \rho \, L_v \, C_E \, U \left(q_{surf} - q_{2m} \right) \qquad \text{------------- (S2)}$$

90
$$Q_B = Q_H \left(1 + 0.6 \, q_{2m} \right) + Q_E \, 0.61 \, \frac{c_p}{L_v} T_{2m} \qquad \text{------------- (S3)}$$

91 where Q_H, Q_E and Q_B surface sensible, latent and buoyancy heat fluxes respectively and S is

92 the dry static energy. S_{surf} is based on the (foundation) GHRSST corrected to be the surface

93 'skin' SST value, and q_{surf} is 98% of the surface saturation humidity (q_{sat}) accounting for the

94 salinity effect. ρ is air density, L_v is the latent heat of vaporization, C_p is the specific heat at

95 constant pressure, U the wind speed accounting the free convection velocity w*, and, C_H and

96 C_E the bulk transfer coefficient for heat and moisture, respectively.

97   Cold-air outbreak conditions were determined in a separate manner for Table S1 and

98   Figure 3. Table S1 classifies an entire flight as either a CAO or a non-CAO flight, based on a

99   visual identification using MODIS imagery from the NASA Worldview URL site

100   (worldview.earthdata.nasa.gov). Days with obscuring cirrus or a lack of low clouds were

101   excluded. For the individual dropsonde analysis shown in Fig. 3, dropsondes were classified

102   as ʻCAOʼ or ʻnon-CAOʼ using the potential difference between the estimated ʻskin

103   GHRSST_skin and that at 900 hPa. This definition emphasizes the surface forcing

104   contribution more than that of the cloud capping inversion than the 850 hPa level applied

105   within Papritz et al., 2015. The lower level was chosen as it clearly avoids falling within the

106   stratiform cloud layer for the deeper boundary layers of the ACTIVATE domain (e.g., Fig.

107   4b, inset).

108

109   Bosilovich, M. G. and Coauthors. (2015). *MERRA-2: Initial evaluation of the climate.*

110   *Technical Report Series on Global Modeling and Data Assimilation*, Vol. 43, NASA Tech.

111   Rep. NASA/TM– 2015–104606, 139 pp. [Available online at

112   https://gmao.gsfc.nasa.gov/pubs/docs/Bosilovich803.pdf.]

113

114   Edson, J. B., Jampana, V., Weller, R.A., Bigorre, S.P., Plueddemann, A.J., Fairall, C.W.,

115   Miller, S.D., Mahrt, L., Vickers, D., & Hersbach, H. (2013). On the exchange of momentum

116   over the open ocean. *Journal of Physical Oceanography*, 43, 1589–1610. doi:10.1175/ JPO-

117   D-12-0173.1.

118   Fairall, C.W., Bradley, E.F., Godfrey, J.S. , Edson, J.B., Young, G.S. and Wick, G.A. (1996)

119   Cool skin and warm layer effects on the sea surface temperature. *J. Geophys. Res., 101,*

120   1295-1308.

121   Hersbach, H., Bell, B., Berrisford, P., et al. (2020). The ERA5 global analysis. *Quarterly*

122   *Journal of Royal Meteorological Society*, 146, 1999-2049. doi:10.1002/qj.3803.

123   Molod, A., Takacs, L., Suarez, M., & Bacmeister, J. (2015). Development of the GEOS-5

124   atmospheric general circulation model: evolution from MERRA to MERRA2. *Geoscientific*

125   *Model Development,* 8, 1339–1356, https://doi.org/10.5194/gmd-8-1339-2015, 2015.

126

127   Papritz, L., Pfahl, S., Sodemann, H., & Wernli, H. (2015). A Climatology of Cold Air

128   Outbreaks and Their Impact on Air–Sea Heat Fluxes in the High-Latitude South Pacific,

129   *Journal of Climate*, *28*, 342-364. doi:10.1175/JCLI-D-14-00482.1

130

131   Reynolds, R.W. & Smith, T.M. (1994). Improved Global Sea Surface Temperature Analysis

132   using Optimum Interpolation. *Journal of Climate*, 7, 929-948. doi: 10.1175/1520-

133   0442(1994)007

134   Rivas, M. B., & Stoffelen, A. (2019). Characterizing ERA-Interim and ERA5 surface wind

135   biases using ASCAT. *Ocean Science*, 15, 831-851. doi: 10.5194/os-15-831-2019

136   Weller, R.A., Bigorre, S.P., Lord, J., Ware, J.D., & Edson, J.B. (2012). A Surface Mooring

137   for Air–Sea Interaction Research in the Gulf Stream. Part I: Mooring Design and

138   Instrumentation. *Journal of Atmosheric and Oceanic Technology*, 29 (9): 1363–1376.

139   doi:10.1175/JTECH-D-12-00060.1

140   Wick, G. A., Hock, T.F., Neiman, P.J., Vömel, H., Black, M.L., & Spackman, J.R.

141   (2018). The NCAR–NOAA Global Hawk Dropsonde System. *Journal of Atmospheric and*

142   *Oceanic Technolology*, 35, 1585–1604. doi:10.1175/JTECH-D-17-0225.1.

143   Wu, W.-S., Purser, R. J., & Parrish, D. F. (2002). Three-dimensional variational analysis

144   with spatially inhomogeneous covariances. *Monthly Weather Review*, 130, 2905–2916,

145   doi:10.1175/ 1520-0493(2002)130,2905:TDVAWS.2.0.CO;2.

146

147

148

149

150

Winter 2020 (mm-dd)	Cloud type (#profiles)	Summer 2020 (mm-dd)	Cloud type (#profiles)
02-14	Cirrus-obscured (4; CAO*)	08-13	non-CAO (5)
02-15	CAO (4)	08-17	non-CAO (6)
02-17	clear (4; non-CAO*)	08-20	non-CAO (5)
02-27	CAO (2)	08-21	non-CAO (5)
02-28	CAO (13)	08-25	non-CAO (6)
02-29	CAO (2)	08-26	non-CAO (6)
03-01	CAO (13)	08-28	non-CAO (8)
03-02	CAO (2)	09-02	non-CAO (6)
03-06	CAO (3)	09-03	non-CAO (6)
03-08	CAO (4)	09-10	non-CAO (4)
03-09	non-CAO (2)	09-11	non-CAO (6)
03-11	non-CAO (2)	09-15	CAO (6)
03-12	non-CAO (4)	09-16	no dropsondes
		09-21	CAO (5)
		09-22	CAO (7)
		09-23	clear (8; non-CAO*)
		09-29	non-CAO (13)
		09-30	non-CAO (5)

151 *CAO under cirrus or non-CAO, using definition of Papritz et al., (2015); $\theta_{SKT} - \theta_{850} > 0$ for CAO.

152

153

154

155

156

157 **Table S1.** Winter and summer 2020 ACTIVATE flight days, cloud conditions and dropsonde
158 number. Eight of the 13 UC-12 King Air flight days in February-March, 2020 sampled
159 cloudy cold-air outbreak (CAO) conditions, encompassing 43 of 59 dropsondes total and 3 of
160 the 18 flight days in August-September 2020, encompassing 18 of 107 dropsondes total).
161 Cloudy CAO conditions were visually determined from satellite imagery and excluded days
162 with obscuring cirrus.

163

164
165
166
167
168
169

CLIMODE		ERA5 - CLIMODE		MERRA2 - CLIMODE		OAFLUX - CLIMODE	
		Feb-Mar	*Aug-Sep*	*Feb-Mar*	*Aug-Sep*	*Feb-Mar*	*Aug-Sep*
BFlux	*Bias*	55	11	39	5	63	5
	RMS	49	15	50	14	54	11
	Correlation	0.85	0.88	0.84	0.86	0.84	0.9
$SST-T_{2m}$	*Bias*	2.1	0.6	0.7	-0.08	1.8	-0.04
	RMS	1.5	0.8	2	0.9	1.7	0.7
	Correlation	0.9	0.85	0.83	0.83	0.88	0.91
$0.98*q_{sat}-q_{2m}$	*Bias*	2.4	2.1	1.2	0.4	2.1	0.8
	RMS	1.2	1.4	1.4	1.5	1.1	1.3
	Correlation	0.83	0.90	0.77	0.89	0.84	0.93
WS_{10m}	*Bias*	0.5	0.13	0.3	-0.35	1.2	-0.03
	RMS	1.7	1.1	1.5	1.4	1.4	1.5
	Correlation	0.90	0.94	0.92	0.91	0.94	0.88

170

171

172 **Table S2**. The mean bias, root mean square (RMS) deviation, and correlation between daily-
173 mean CLIMODE buoy and ERA5, MERRA2 and OAFLUX values of buoyancy flux (W m^{-2}),
174 SST-T_{2m} (K), $0.98*q_{sat}-q_{2m}$ (g kg^{-1}), and WS_{10m} (m s^{-1}) depicted for February-March and
175 August-September in 2006.

176
177
178
179
180
181

182

183

ACTIVATE		ERA5 - ACTIVATE		MERRA2 - ACTIVATE	
		Feb-Mar	*Aug-Sep*	*Feb-Mar*	*Aug-Sep*
SHF	*Bias*	-2.5	-0.24	-22.8	-4.84
	RMS	41	9.62	30	10.12
	Correlation	0.93	0.97	0.95	0.97
LHF	*Bias*	-4	-19.61	-58	-31.12
	RMS	106.5	54.88	86.5	58.67
	Correlation	0.81	0.94	0.87	0.95
SST-T_{2m}	*Bias*	-0.2	0.32	-1.15	-0.26
	RMS	0.91	0.66	1.03	0.50
	Correlation	0.97	0.93	0.96	0.96
$0.98*q_{sat}-q_{2m}$	*Bias*	-0.16	0.45	-1.35	-0.87
	RMS	1.06	1.25	1.05	1.23
	Correlation	0.89	0.93	0.93	0.94
WS_{10m}	*Bias*	-0.12	-0.47	-0.97	-0.92
	RMS	1.99	1.17	2.02	1.31
	Correlation	0.89	0.9	0.88	0.87
Inversion top height	*Bias*	-74	-205	-96	-186
	RMS	-375	-425	-323	-587
	Correlation	0.83	0.62	0.89	0.48

184

185

186 **Table S3**. The mean bias, root mean square (RMS) deviation, and correlation between
187 ACTIVATE dropsonde and ERA5/MERRA2 values of sensible and latent heat fluxes (SHF
188 and LHF respectively, W m^{-2}), SST-T_{2m} (K), $0.98*q_{sat}-q_{2m}$ (g kg^{-1}), WS_{10m} (m s^{-1}), and the
189 inversion top height (m), estimated using a relative humidity threshold for February-March
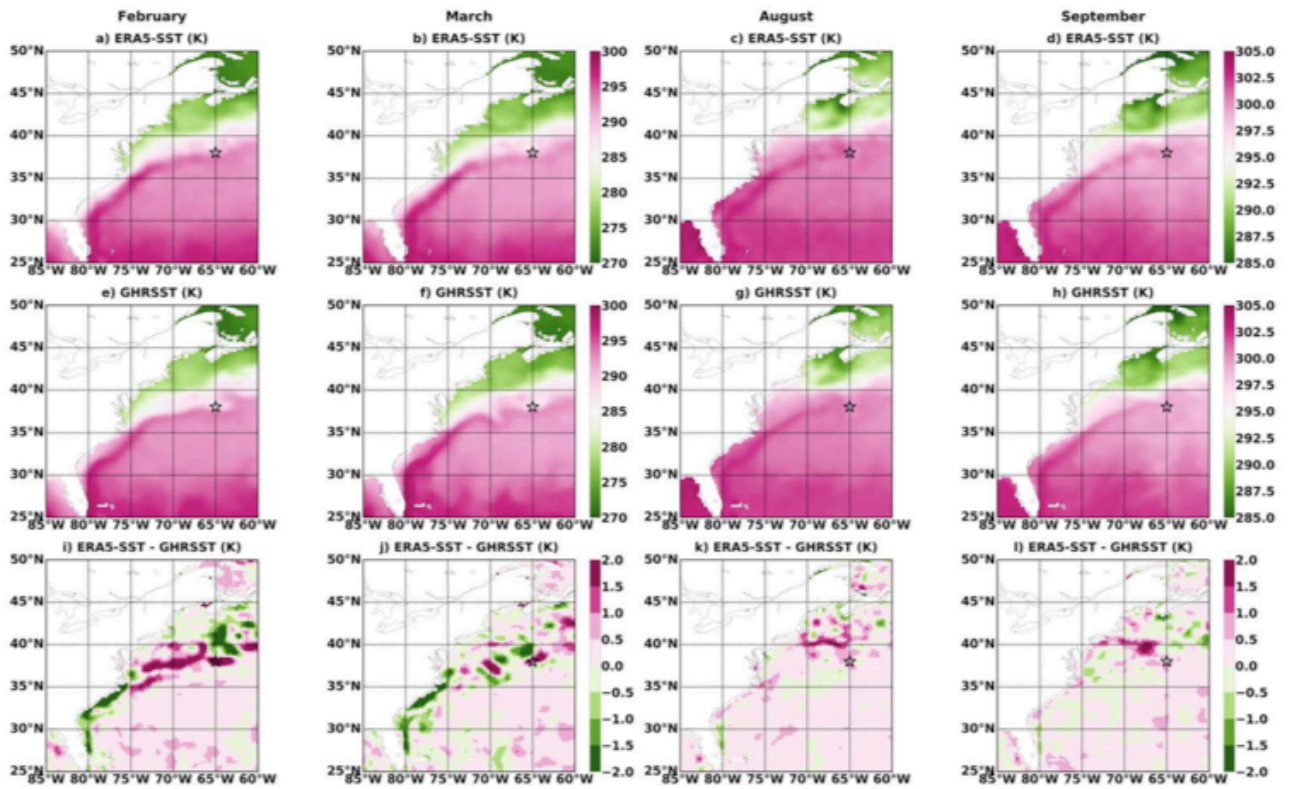190 and August-September in 2020.

191
192
193
194
195
196
197

198

Figure S1. Top row: ERA5 foundation SST spatial distribution during February, March, August, and September in 2006. Middle row: same as top but for GHRSST. Bottom row: (ERA5-SST – GHRSST) difference for the same four months.
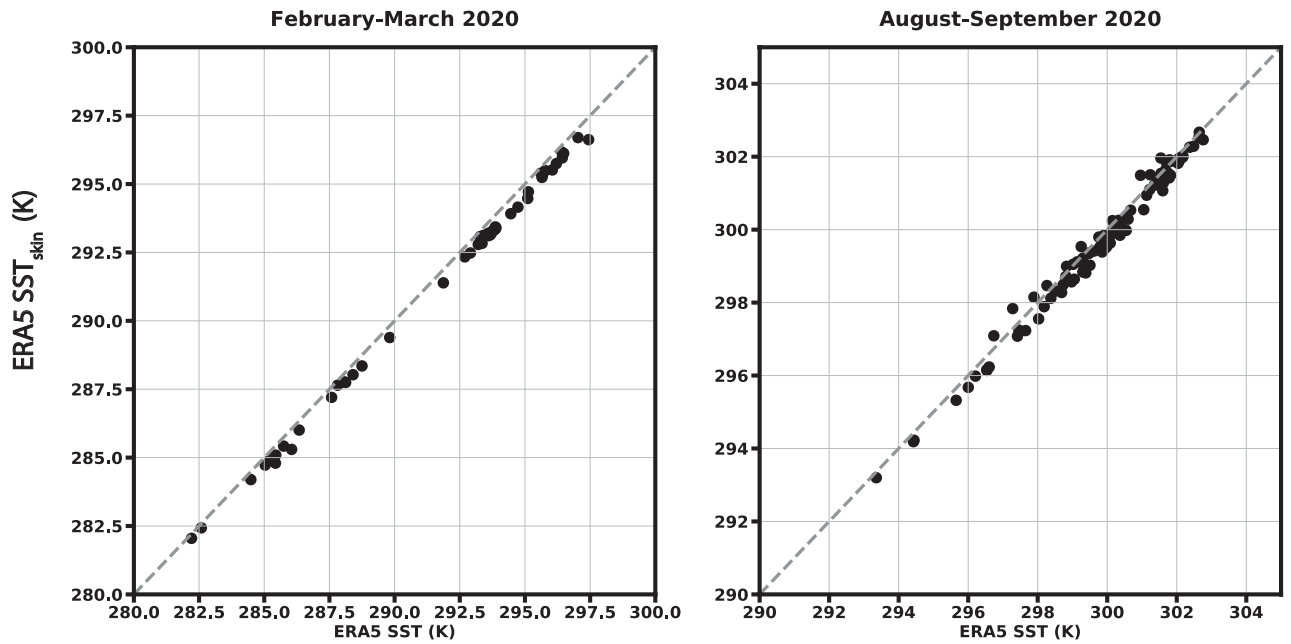
February-March 2020   **August-September 2020**

205

206

207 **Figure S2.** ERA5 skin sea surface temperature (SST_{skin}) as a function of its foundation SST
208 at 1-m depth, at dropsonde locations and times for left) February-March 2020 and right)
209 August-September 2020.

210

Figure S3. Monthly-means at the CLIMODE buoy in year 2006 of a) buoyancy flux, b) SST and T_{2m}, c) 0.98*q_s and q_{2m}, and d) 10 m wind speed (WS_{10m}) for the CLIMODE buoy (black), ERA5 (red), MERRA2 (green), and OAFLUX (yellow). MERRA2 SST is a skin value, while the buoy, ERA5, and OAFLUX SSTs are foundation SSTs. OAFLUX WS_{10m} is the neutral wind speed.
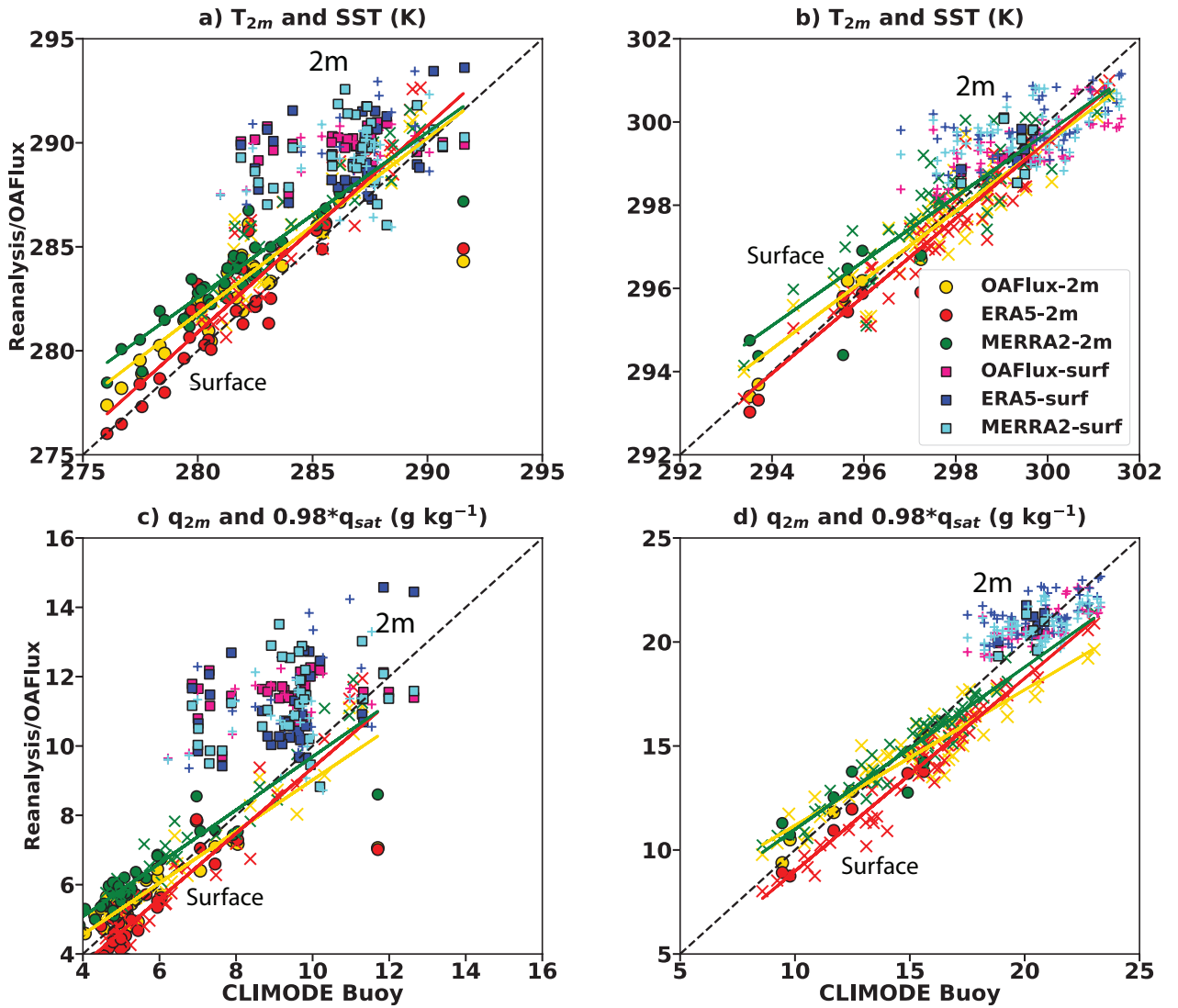
Figure S4. Comparison of ERA5, MERRA2 and OAFLUX daily mean surface meteorology against left) CLIMODE buoy for February-March 2006 a) SST and T_{2m}, and c) q_s and q_{2m}. Right two panels are the same as the left panels but for August-September 2006. The filled circles represent the days with cold-air outbreak conditions, whereas 'x' denotes non-CAO days.
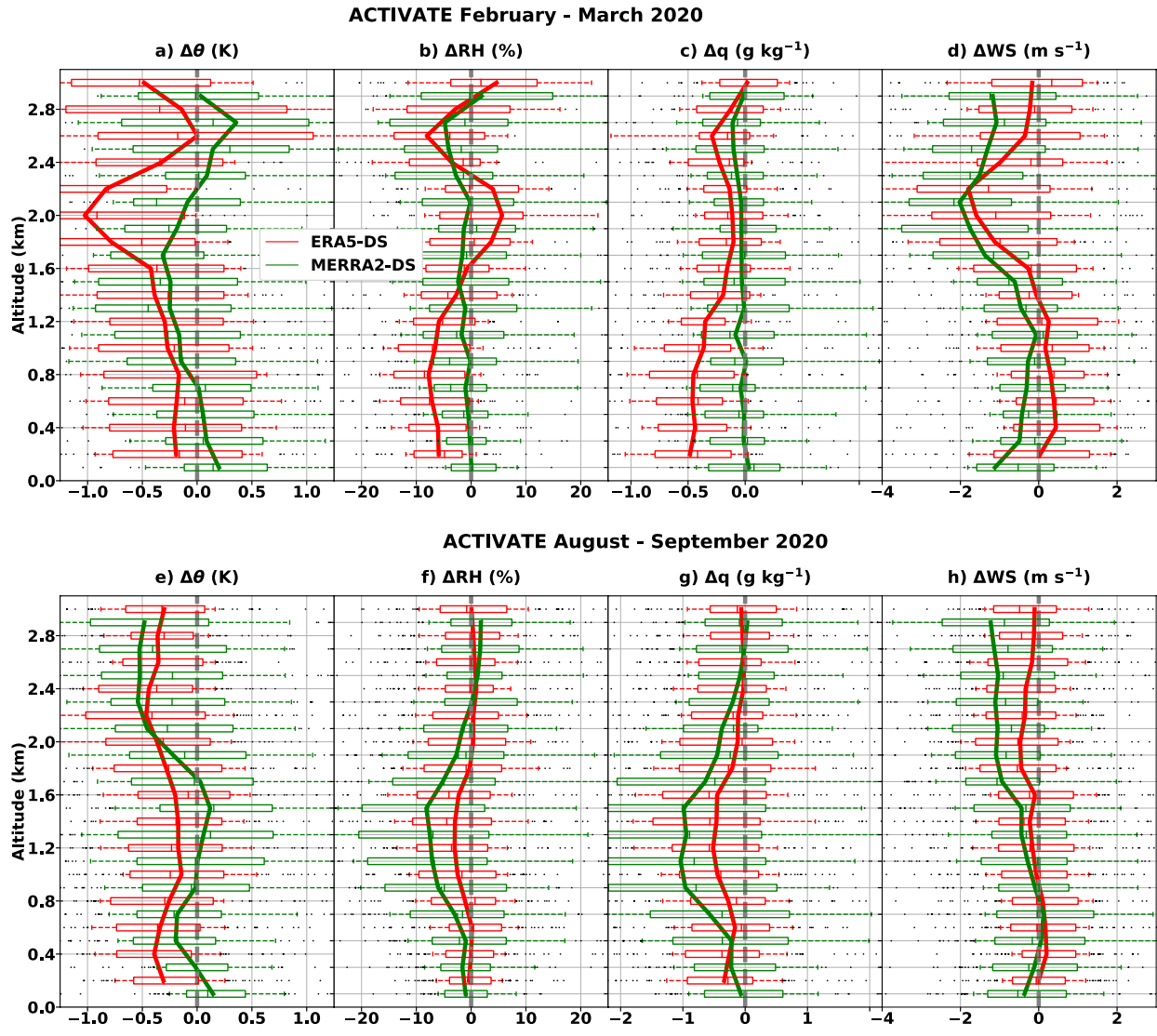
Figure S5. Mean difference between dropsondes and reanalysis profiles (ERA5 in red and MERRA2 in green; reanalysis-dropsonde) in a) potential temperature, b) relative humidity, c) specific humidity, and d) wind speed of February-March 2020, shown as the interquartile range (horizontal bars), 15–85 percentile (thin horizontal dashed line), and median (thin vertical line). e)-h): same as a)-d) but for August-September 2020 deployment.